An Extended Least Squares Method for Aliasing-Resistant Vector Velocity Estimation

Ingvild Kinn Ekroll, *Member, IEEE*, Jørgen Avdal, *Member, IEEE*, Abigail Swillens, Hans Torp, *Member, IEEE*, and Lasse Løvstakken, *Member, IEEE*

***Abstract*— An extended least squares method for robust, angle-independent 2-D vector velocity estimation using plane-wave ultrasound imaging is presented. The method utilizes a combination of least squares regression of Doppler autocorrelation estimates and block matching to obtain aliasing-resistant vector velocity estimates. It is shown that the aliasing resistance of the technique may be predicted using a single parameter, which is dependent on the selected transmit and receive steering angles. This parameter can therefore be used to design the aliasing-resistant transmit–receive setups. Furthermore, it is demonstrated that careful design of the transmit–receive steering pattern is more effective than increasing the number of Doppler measurements to obtain robust vector velocity estimates, especially in the presence of higher order aliasing. The accuracy and robustness of the method are investigated using the realistic simulations of blood flow in the carotid artery bifurcation, with velocities up to five times the Nyquist limit. Normalized root-mean-square (rms) errors are used to assess the performance of the technique. At −5 dB channel data blood SNR, rms errors in the vertical and horizontal velocity components were approximately 5% and 15% of the maximum absolute velocity, respectively. Finally, the *in vivo* feasibility of the technique is shown by imaging the carotid arteries of healthy volunteers.**

***Index Terms*— Aliasing-resistant estimator, least mean square algorithms, ultrasound blood flow imaging, vector velocity estimation.**

I. Introduction

TWO-DIMENSIONAL (2-D) vector velocity imaging has the potential to visualize complex blood flow patterns in the ultrasound imaging plane. For blood flow velocity quantification, the utilized technique should also provide accurate, angle-independent velocity estimates and cover a large velocity span.

Vector Doppler (VD) imaging is one approach to angle-independent velocity estimation, in which the Doppler measurements from multiple intersecting ultrasound beams are combined to form vector velocity estimates. This approach was investigated using different transmit–receive configurations of single-element transducers already in the 1970s, and after the introduction of ultrasonic arrays and beam steering, a multitude of VD strategies has been proposed [1]. The number of intersecting ultrasound beams and how they are combined to provide 2-D estimates vary between techniques, ranging from the split aperture approach, using a single transmit direction and two separate receive apertures [2], [3], to least mean squares regression of multiple Doppler measurements [4]. An approach similar to the split aperture approach is the transverse oscillation technique [5], where apodization windows are applied on receive to produce a laterally oscillating field using a single transmit direction. Maniatis *et al.* [6] investigated different strategies for 2-D velocity reconstruction in a simulation study, and concluded that the dominant factor determining the velocity estimation accuracy is the angle between the observation directions. They also concluded that multidirectional (more than two) measurements might be beneficial in conditions where the true flow velocity direction is unknown.

Two-dimensional spatial information available from parallel receive beamforming has enabled other vector velocity estimation methods, including blood speckle tracking [7] and directional beamforming [8]. Recently, the established VD techniques have also been reapplied using plane-wave transmissions to visualize 2-D flow patterns in a larger field of view [9], [10].

VD imaging based on the autocorrelation technique is hampered by aliasing, as the maximum velocity that can be unambiguously measured is limited by the pulse repetition frequency (PRF). Because the maximum PRF is ultimately restricted by the imaging depth, this leads to a compromise between the measurable velocity span and the number of transmit beams that can be used to generate the velocity vectors. Methods using more than one transmit beam [4], [11] have the potential to increase the accuracy of VD by increasing the angle between observations, but on the cost of a smaller measurable velocity span due to the reduced Doppler PRF. In pathological flow situations, e.g., when grading a carotid stenosis, the velocities can be higher than 2.3 m/s [12], in which case aliasing may also occur when using the maximum Doppler PRF.

Aliasing is a problem with proposed solutions in many fields, such as synthetic aperture radar [13] and audio processing [14]. In the field of medical ultrasound and Doppler blood flow imaging, several methods have been proposed addressing the velocity ambiguity problem, including methods using *a priori* assumptions about the flow field [15]–[17] such as smoothness and continuity. In [18], a staggered PRF

Manuscript received May 30, 2016; accepted July 11, 2016. Date of publication July 14, 2016; date of current version November 1, 2016.

I. K. Ekroll is with the Department of Circulation and Medical Imaging, Norwegian University of Science and Technology, Trondheim 7491, Norway, and also with St. Olav Hospital, Trondheim University Hospital, Trondheim 7030, Norway (e-mail: ingvild.k.ekroll@ntnu.no).

J. Avdal, H. Torp, and L. Løvstakken are with the Norwegian University of Science and Technology, Trondheim 7491, Norway (e-mail: jorgen.avdal@ntnu.no; hans.torp@ntnu.no; lasse.lovstakken@ntnu.no).

A. Swillens is with Ghent University, Ghent 9000, Belgium (e-mail: abigail.swillens@ugent.be).

This paper has supplementary downloadable material available at http://ieeexplore.ieee.org., provided by the author.

Digital Object Identifier 10.1109/TUFFC.2016.2591589

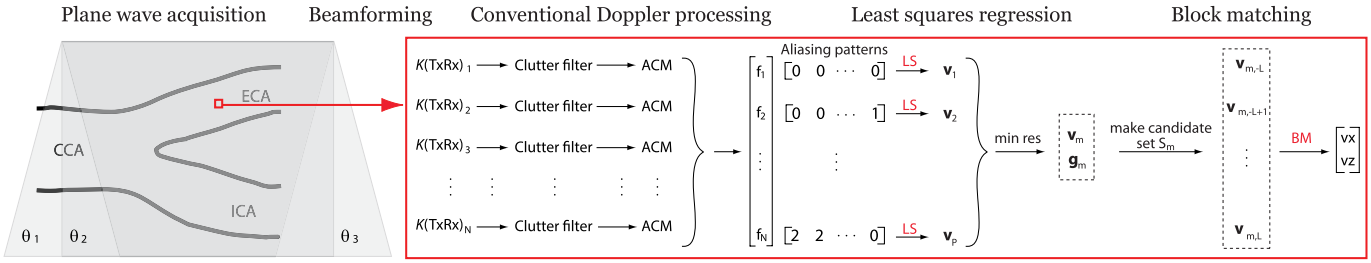

Fig. 1. Using a small number of transmit angles and the design scheme detailed in Section II-D to determine the tx/rx patterns, N Doppler autocorrelation estimates are generated for every image pixel in the overlap region. A least squares estimator accounting for potential aliasing produces a set of candidate velocity vectors as explained in Section II-A. Ambiguities are resolved by BM between successive (coherently compounded) frames in the Doppler ensemble (see Section II-B).

acquisition was used to extend the measurable velocity span of Doppler ultrasound to several times the Nyquist limit, whereas Yiu *et al.* [10] performed aliasing correction on individual Doppler shifts before calculating the VD estimates using least squares regression. Recently, an aliasing-resistant VD method was presented by Flynn *et al.* [19], [20], where single-wrap aliasing ambiguities are resolved by solving a least squares problem for all probable aliasing configurations and selecting the solution with the smallest residual.

Based on the principle of solving multiple least squares problems as presented in [19], we propose a method to increase the robustness of the aliasing pattern selection and to ensure resistance to higher order aliasing. This is achieved by, first, extending the method in [19] to include multiple receive beam directions for each transmission. Theory enabling quantification of aliasing resistance is developed, and is further used to obtain aliasing-resistant transmit and receive angle combinations. Finally, we show that the least squares VD technique cannot reliably distinguish aliasing patterns for higher order aliasing and propose to resolve such ambiguities using a computationally cheap block matching (BM) scheme. The resulting method, from now on referred to as extended least squares VD (ELS-VD), can be used to produce aliasing-resistant 2-D velocity estimates from a single plane-wave transmission, but also allows for improved accuracy of vector velocity estimates by increasing the number of transmit angles without reducing the measurable velocity span. The robustness of the method is shown through theoretical analysis, simulations, and *in vivo* experiments.

Sections II-A–II-C provide the theoretical framework for the proposed method, whereas Sections II-D and II-E focus on practical implementation. Sections II-F and II-G describe the complex flow simulation study and the *in vivo* feasibility study, respectively. Aliasing-resistant transmit–receive setups suited for vascular imaging are presented in Section III-A. The performance of the proposed technique is assessed in Sections III-B and III-C, whereas Sections III-D and III-E provide the *in vivo* examples from healthy volunteers. A discussion of the results follows in Section IV. Finally, this paper is concluded in Section V.

II. Methods

Fig. 1 provides an overview of the acquisition and processing, which produces the vector velocity estimates from channel data. Building on conventional (pixel-based) beamforming and Doppler (autocorrelation) processing, the novel parts of the algorithm are described in Sections II-A–II-D. The three parts of the algorithm are: selecting transmit–receive angle patterns with high aliasing resistance (Sections II-C and II-D), finding the aliasing patterns and velocity vector candidates yielding the smallest least squares residuals (Section II-A), and, finally, resolving aliasing ambiguities and determining the true 2-D velocity vector using block matching (Section II-B).

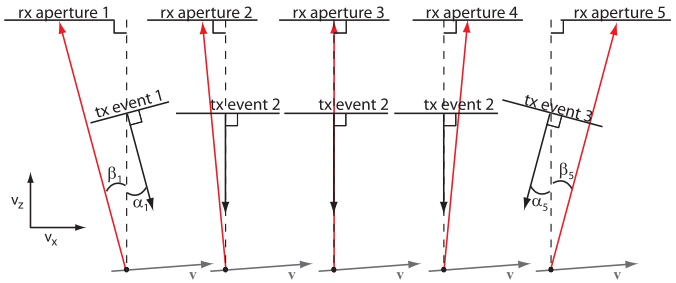

Fig. 2. Example of transmit and receive geometry for a single image point, which is successively insonated by three plane waves of different steering angles. In this example, receive beamforming is done for five different directions (red arrows) in total. Each transmit event has been paired with one or more receive steering angles, yielding five unique two-way Doppler angles. Transmit–receive angle pair n has the steering angles (α_n and β_n).

A. Vector Doppler: Least Squares Regression

The area of interest is insonated from a small ($M = 1 - 5$) number of transmit angles, fired successively as in a coherent compounding setup. For each resolution cell in the ultrasound image, the Doppler frequency is estimated for N different transmit–receive (TxRx) angle combinations, each corresponding to a unique two-way Doppler angle. The transmit–receive geometry for a single image point is shown in Fig. 2. The velocity vector $\boldsymbol{v} = [v_x, v_z]$ corresponding best to the measured Doppler shifts can then be found by solving a least squares problem. However, to account for potential aliasing in the estimates of one or more of the N Doppler frequencies, separate least squares problems are solved for all possible aliasing patterns. Similar to the approach in [19], each least squares problem can be written in the form

$$k\boldsymbol{A}\boldsymbol{v}_i = \hat{\boldsymbol{f}} + \boldsymbol{g}_i \tag{1}$$

where i iterates through all the aliasing patterns and their corresponding solutions, k is a constant factor converting velocity to normalized frequency, $\hat{\boldsymbol{f}} = [f_0 \dots f_{N-1}]^T + \boldsymbol{\epsilon}$ is a vector containing normalized Doppler frequency estimates from N different TxRx combinations, and $\boldsymbol{\epsilon}$ represents the measurement noise. The matrix $\boldsymbol{A} = \boldsymbol{A}_{tx} + \boldsymbol{A}_{rx}$ has dimensions

$N \times 2$, and is the sum of the projection matrices onto the transmit and receive Doppler directions, respectively. The rows of $\boldsymbol{A}$ are given by

$$\boldsymbol{a}_n = [-\sin\alpha_n - \sin\beta_n, \cos\alpha_n + \cos\beta_n] \tag{2}$$

where α_n and β_n are the steering angles of the angle pair n on transmit and receive, respectively. The aliasing vectors $\boldsymbol{g}_i$ are the corrections to $\hat{\boldsymbol{f}}$ for all aliasing pattern candidates, and all the elements in these vectors represent a frequency bias of an integer number of PRFs. In this paper, $\boldsymbol{g}_i$ runs through all the combinations of integers with absolute value smaller than L. The parameter L represents the maximum aliasing order to be investigated and depends on the application's Doppler PRF and the expected maximum velocity.

The general least squares solutions to (1) are on the form

$$\boldsymbol{v}_i = k^{-1}\boldsymbol{A}_W^{+}(\hat{\boldsymbol{f}} + \boldsymbol{g}_i) \tag{3}$$

where

$$\boldsymbol{A}_W^{+} = (\boldsymbol{A}^T\boldsymbol{W}\boldsymbol{A})^{-1}\boldsymbol{A}^T\boldsymbol{W}. \tag{4}$$

The weighting matrix $\boldsymbol{W}$ is typically used to account for differences in the variances of the autocorrelation estimates. In this paper, we will use uniform weighting, and thus $\boldsymbol{W} = \boldsymbol{I}$, but the matrix is still included in the expressions for completeness. For each solution $\boldsymbol{v}_i$ of (1), (3) can be used to calculate the least squares residual

$$\begin{aligned} r_i &= \|\boldsymbol{W}^{1/2}(k\boldsymbol{A}\boldsymbol{v}_i - (\hat{\boldsymbol{f}} + \boldsymbol{g}_i))\|_2 \\ &= \left\|\boldsymbol{W}^{1/2}\left(\boldsymbol{A}\boldsymbol{A}_W^{+} - \boldsymbol{I}\right)(\hat{\boldsymbol{f}} + \boldsymbol{g}_i)\right\|_2. \end{aligned} \tag{5}$$

The solution $\boldsymbol{v}_m$ with the smallest residual r_m is selected as the dealiased solution.

B. Block Matching: Resolving Ambiguities

A notable drawback of the method described in Section II-A is that it cannot reliably distinguish the two candidate vector solutions $\boldsymbol{v}_i$ and $\boldsymbol{v}_j$ if the difference between their respective residuals r_i and r_j is small compared with the norm of the measurement noise $\boldsymbol{\epsilon}$. Moreover, it follows from the triangle inequality that the difference between r_i and r_j has an upper bound given by:

$$|r_j - r_i| \le B_{ij} \tag{6}$$

where

$$B_{ij} = \left\|\boldsymbol{W}^{1/2}\left(\boldsymbol{A}\boldsymbol{A}_W^{+} - \boldsymbol{I}\right)(\boldsymbol{g}_j - \boldsymbol{g}_i)\right\|_2. \tag{7}$$

The relation between the residuals r_i, r_j, and B_{ij} is shown in Fig. 3. Note that when $\boldsymbol{W} = \boldsymbol{I}$, B_{ij} is independent of the measured data. It follows from (6) that a small value of B_{ij} leads to increased probability of selecting $\boldsymbol{g}_j$ in pixels where the correct aliasing pattern is $\boldsymbol{g}_i$, and vice versa. Thus, the solutions $\boldsymbol{v}_i$ and $\boldsymbol{v}_j$ will be indistinguishable if B_{ij} is small.

In practice, when $\cos\alpha_n \approx 1$ for all steering angles, B_{ij} is very small (<0.005) if

$$\boldsymbol{g}_j = \boldsymbol{g}_i + [l, l, \ldots, l] \tag{8}$$

where l is an integer and $|l| \le L$. In the extreme case $B_{ij} = 0$, the method will select $\boldsymbol{g}_i$ and $\boldsymbol{g}_j$ with equal probability.

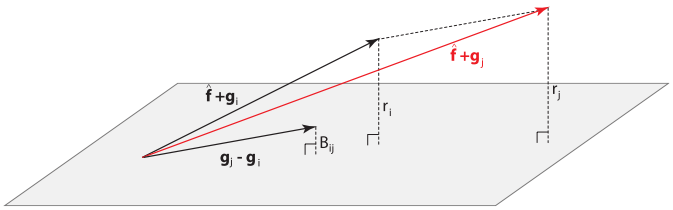

Fig. 3. Shaded area shows the plane spanned by the columns of $\boldsymbol{A}$. The measurement vector $\hat{\mathbf{f}}$ yields the two residuals r_i and r_j when combined with the two aliasing vectors $\boldsymbol{g}_i$ and $\boldsymbol{g}_j$. Note that in the case where the vector $\boldsymbol{g}_i - \boldsymbol{g}_j$ is in the plane, we have $B_{ij} = 0$ and $r_i = r_j$, and the two solutions $\boldsymbol{v_i}$ and $\boldsymbol{v_j}$ are indistinguishable.

As a consequence, any solution $\boldsymbol{v}_i$ actually belongs to a set S_i of up to $2L + 1$ vectors that are in practice indistinguishable using the least squares approach. We define S_i to be the set of candidate vector solutions $\boldsymbol{v}_{i,l}$ to (5) with aliasing patterns $\boldsymbol{g}_{i,l}$, given by

$$\boldsymbol{g}_{i,l} = \boldsymbol{g}_i + [l, l, \ldots, l], \quad \max|\boldsymbol{g}_{i,l}| \le L. \tag{9}$$

In this paper, least squares regression is used to select the set S_m containing the velocity vector candidates with the smallest residuals. The above analysis shows, however, that least squares regression alone is not sufficient to distinguish different candidates in S_m. To select the best candidate in S_m, we propose to use spatiotemporal cross correlation. The normalized cross correlation is measured for all the velocity vectors in the set S_m. The candidate vector with the highest correlation is selected. The BM step also functions as validation of the vector velocity estimates, and estimates with correlation values below 0.1 are excluded.

1) A Vector Velocity Ambiguity Example: In a case with $N = 5$ and $L = 2$, the minimal r_m in (5) is found for velocity vector $\mathbf{v}_m$ with corresponding aliasing pattern $\mathbf{g}_m = [0, 1, 1, 1, 2]$. The set S_m now consists of velocity vectors with the aliasing patterns $[-1, 0, 0, 0, 1]$, $[-2, -1, -1, -1, 0]$, and $[0, 1, 1, 1, 2]$. The residuals of the three velocity vectors are approximately equal. Therefore, the spatial cross correlations of all the candidates in S_m are calculated. The velocity vector candidate with the highest correlation becomes the selected candidate.

C. Aliasing-Resistant Transmit–Receive Patterns: Properties

In the previous section, it was shown that two candidate vectors in the same set are in practice indistinguishable by least squares regression alone, because the corresponding B_{ij} is small. Without further precautions, ambiguities may also arise between the correct vector v_i and a candidate v_j from a different set. In the following, however, we show that a large value of B_{ij} implies that the least squares step will select the correct candidate v_i with high probability. To understand this, it is useful to consider the scenario without measurement bias or noise. In this case, the residual r_i and the aliasing pattern g_i corresponding to v_i fulfill

$$r_i = \left\|\boldsymbol{W}^{1/2}\left(\boldsymbol{A}\boldsymbol{A}_W^{+} - \boldsymbol{I}\right)(\hat{\boldsymbol{f}} + \boldsymbol{g}_i)\right\|_2 = 0 \tag{10}$$

TABLE I
FREQUENTLY USED VARIABLES WITH A SHORT SUMMARY OF DEFINITIONS

Variable	Definition	Variable	Definition
$\mathbf{A}$	Sum of Tx and Rx projection matrices	$\mathbf{f}$	Doppler measurement vector
$\mathbf{g}_i$	Aliasing vector	$\mathbf{W}$	Measurement weighting matrix
r_i	Least squares residual	B_{ij}	Upper bound for residual difference
$\min B_{ij}$	Measure of aliasing resistance for a given TxRx combination	L	Maximum aliasing order
S_i	Set of candidate velocity vectors indistinguishable by LS method	K	Doppler ensemble length
N	Number of TxRx pairs and unique Doppler angles in a combination	M	Number of plane wave transmissions

and the incorrect aliasing pattern g_j will yield the residual

$$\begin{aligned} r_j &= \left\| \boldsymbol{W}^{1/2}\left(\boldsymbol{A}\boldsymbol{A}_W^{+} - \boldsymbol{I}\right)(\hat{\boldsymbol{f}} + \boldsymbol{g}_j)\right\|_2 \\ &= \left\| \boldsymbol{W}^{1/2}\left(\boldsymbol{A}\boldsymbol{A}_W^{+} - \boldsymbol{I}\right)(\hat{\boldsymbol{f}} + \boldsymbol{g}_i + (\boldsymbol{g}_j - \boldsymbol{g}_i))\right\|_2 \\ &= \left\| \boldsymbol{W}^{1/2}\left(\boldsymbol{A}\boldsymbol{A}_W^{+} - \boldsymbol{I}\right)(\boldsymbol{g}_j - \boldsymbol{g}_i))\right\|_2 = B_{ij}. \end{aligned} \tag{11}$$

The method will only select the erroneous aliasing pattern candidate g_j if $r_j < r_i$, meaning that the impact of noise and bias must change the value of $r_j - r_i$ from B_{ij} to something negative. This becomes unlikely when B_{ij} is large compared with the standard deviation and bias of the frequency estimates.

Based on the above analysis, the method will select the correct velocity vector candidate v_i with high probability if all the possible values of B_{ij} are large. Thus, the value of the minimum B_{ij} qualifies as a parameter which describes how aliasing-resistant a given combination of transmit and receive steering angles is, when utilized in least squares VD. Increased aliasing resistance may be ensured by selecting the transmit and receive angles such that the minimum B_{ij} is as large as possible.

1) Another Vector Velocity Ambiguity Example: In a setup with five transmit angles $[-10°, -5°, 0°, 5°, 10°]$, all beamformed with 0° steering on receive, the correct velocity vector is $\boldsymbol{v}_i = [v_x, v_z]$, with corresponding aliasing pattern g_i and residual $r_i = 0$ (no noise or bias). If the Nyquist velocity is $\boldsymbol{v}_N$, then the velocity vector $\boldsymbol{v}_j = [v_x - 2v_N/\sin 10, v_z]$ has the aliasing pattern $\boldsymbol{g}_j = g_i + [-2, -1, 0, 1, 2]$ and the residual $r_j = 0.005$. The velocity vectors $\boldsymbol{v}_i$ and $\boldsymbol{v}_j$ are not in the same set, but the corresponding $B_{ij} = 0.005$ is low. Thus, we have a significant probability of selecting the erroneous candidate $\boldsymbol{v}_j$ in the presence of noise, when using the least squares regression with this setup.

D. Aliasing-Resistant Transmit–Receive Patterns: Design

For any given transmit–receive pattern, the minimum value of B_{ij} is obtained by evaluating (7) for all possible values of $\boldsymbol{g}_j - \boldsymbol{g}_i$. The pairs $[\boldsymbol{g}_i, \boldsymbol{g}_j]$ fulfilling (8) are excluded, as these cases are resolved using BM. The transmit–receive pattern with largest minimum B_{ij} is found by discretizing the set of all transmit–receive combinations and calculating the minimum B_{ij} for each pattern.

In this paper, the following additional restrictions were imposed for the selection of the transmit–receive combinations. Note that these restrictions are only utilized to allow design of aliasing-resistant transmit–receive patterns according to user preferences, which can be both application and probe/geometry dependent:

1) maximal angle span equal to 30 degrees;
2) symmetry with respect to the axial axis;
3) at most 3 Tx angles, to maintain a high Doppler PRF;
4) at most 7 TxRx combinations, to limit the computational cost.

The requirements 1) to 3) force the Tx angles to be −15°, 0°, or 15°. We allowed the Rx angles to be chosen from 121 equally spaced values in the interval $[-15°, 15°]$. With these restrictions, all possible combinations with five and seven angle pairs were generated. For each combination, all the values of B_{ij} were calculated using (7) with a uniform weighting function $\boldsymbol{W}$. The transmit–receive combinations with the largest minimum B_{ij} were selected. Using a uniform weighting function ensures that the optimization is not data dependent, as the matrix $\boldsymbol{A}$ in (7) is dependent on the transmit–receive pattern only. The result is, however, dependent on the maximum allowed aliasing order, as this determines the span of $\boldsymbol{g}_i$ and $\boldsymbol{g}_j$.

E. Implementation and Computational Cost

To reduce the computational cost of the method, only one representative from each set S_i was evaluated when performing the least squares regression in Section II-B. This was achieved by selecting the aliasing patterns $\boldsymbol{g}_i$ with central element zero. In addition, the number of aliasing patterns was restricted by requiring that the difference between the largest and smallest element in g_i was ≤ 2. With these restrictions, we had to solve 3^{2L} least squares problems and perform $(2L+1)(K-1)$ cross correlations with kernel size P for each pixel in the image, where K is the number of frames in a Doppler ensemble. In a setup with $L = 2$, $K = 50$, $P = 25$, and 256×256 VD estimates, each vector velocity image was calculated in less than 5 s in a MATLAB (Mathworks, Natick, and MA) environment running on a 2.7-GHz Intel i7-4800MQ processor (least squares regression) and an NVIDIA Quadro 4100M GPU (BM). BM was performed on the image series generated by coherent compounding of the low resolution images from the M different transmit angles. In the cases where $M = 1$, BM was performed on a single low resolution image.

F. Simulation Study

A scatterer phantom was created based on the patient specific fluid-structure interaction (FSI) simulations,

TABLE II
ACQUISITION AND BEAMFORMING SPECIFICATIONS

Simulations	
Active transmit elements	192
Pitch [μm]	230
Transmit (Tx) freq. [MHz]	5.7
Doppler PRF Case 1 [kHz]	4
Doppler PRF Case 2 [kHz]	2
Ensemble length Case 1	100
Ensemble length Case 2	50
Polynomial filter order Case 1	10
Polynomial filter order Case 2	6
Channel data SNR, [dB]	[-15, -14, -13, -12, -10, -8, -5, 10]
In vivo 1	
Shorthand name	L12
Active transmit elements	128
Pitch [μm]	200
Transmit (Tx) freq. [MHz]	8.9
Doppler PRF [kHz]	3
In vivo 2	
Shorthand name	L11
Active transmit elements	128
Pitch [μm]	300
Transmit (Tx) frequency [MHz]	6.25
Doppler PRF [kHz]	3
General	
Probe type	Linear array
Pulse periods	2.5
Receive (Rx) F#	1.4
Number of transmit angles	1, 2 or 3
Transmit angles, α_n [deg]	[-15, 0, 15]
Receive angles, β_n [deg]	See Table III

TABLE III
TRANSMIT–RECEIVE PATTERNS WITH LOW (1–3) AND HIGH (4–7) ALIASING RESISTANCE

Pattern	TxRx pairs [deg]	min B_{ij}
1	[-15, -15, 0, 15, 15] [-15, 0, 0, 0, 15]	$2.9 \cdot 10^{-16}$
2	[-15, -15, 0, 0, 0, 15, 15] [-15, 0, -15, 0, 15, 0, 15]	$7.6 \cdot 10^{-16}$
3	[-15, -15, -15, 0, 0, 0, 15, 15, 15] [-15, 0, 15, -15, 0, 15, -15, 0, 15]	$6.6 \cdot 10^{-16}$
4	[-15, 0, 0, 0, 15] [-15, -10, 0, 10, 15]	0.44
5	[-15, -15, 0, 0, 0, 15, 15] [-15,-3.75,-8.75, 0, 8.75, 3.75, 15]	0.65
6	[-15, -15, -15, -15, 15, 15, 15] [-15, -3, 6, 15, -6, 3, 15]	0.65
7	[0, 0, 0, 0, 0, 0, 0] [-15, -9.5, -5, 0, 5, 9.5, 15]	0.65

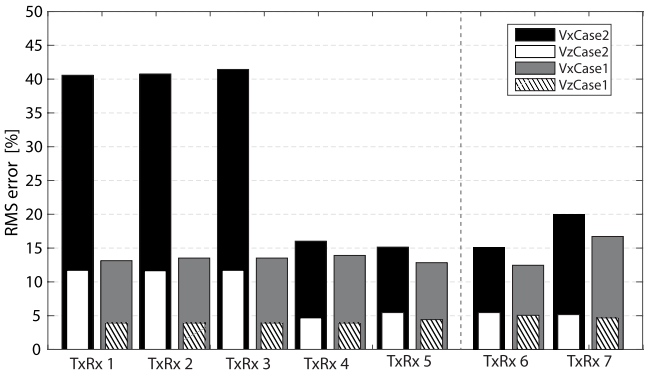

Fig. 4. Bars show the normalized rms errors of the estimated horizontal and vertical velocity components for the simulation case 1 (PRF = 4 kHz) and case 2 (PRF = 2 kHz), using all the transmit–receive patterns given in Table I.

where the 3-D geometry was reconstructed from Computed Tomography (CT) scans of a stenosed carotid bifurcation [21]. As detailed in the work by Swillens *et al.* [21], fully developed flow in the region of interest (the bifurcation) was ensured by artificially prolonging the in- and outlets, and physiologically realistic boundary conditions were applied. The output of the FSI simulations was then coupled with the Field II software [22], as described in [23], to generate ultrasound channel data. Simulations included both the vessel wall and fluid (blood) scatterers. This was done to have a realistic, high velocity flow field with a known ground truth, also containing nonstationary clutter from tissue scatterer side-lobes. To create fully developed speckle in the vessel lumen, ten scatterers were used per resolution cell. Structured scatterers were utilized to mimic the reflections at the intima and adventitia layers [23]. In the fluid domain, continuous scatterer generation was ensured by giving all the scatterers a life span of 25 ms, with 20% being regenerated every 5 ms. White noise was added to the channel data to emulate different levels of thermal noise (Table II). Beamforming and coherent summation of three low resolution images resulted in blood SNRs from 2.7 to 23 dB. The amplitudes of the tissue scatterers were adjusted to give a clutter-to-blood ratio in the vessel lumen of 30 dB after beamforming. Delay-and-sum beamforming was performed using in-house code with the parameters found in Table II, and a polynomial regression (high pass) filter was applied to the N Doppler ensembles separately, with a -6 dB cutoff at 1.5 cm/s. Autocorrelation estimates were averaged in a region of 0.8 mm $\times$ 0.8 mm. A temporal window of 25 ms in peak systole was simulated, and the results from two cases will be presented.

Case 1 (Single-Wrap Aliasing): The maximum measured Doppler velocity was close to 2.5 times the Nyquist limit.

Case 2 (Double-Wrap Aliasing): The Doppler PRF was halved, resulting in a maximum Doppler velocity just below 5 times the Nyquist limit.

A 2-D plane corresponding to the Field II ultrasound imaging plane was extracted from the 3-D FSI velocity field and utilized as ground truth, depicting the flow field in peak systole for that specific patient (geometry and boundary conditions) and ultrasound imaging plane. To assess the performance of the proposed method, the estimated vector velocity field was compared with the ground truth by calculating the normalized root-mean-square (rms) errors for each of the two velocity components in every pixel. The rms errors were normalized with respect to the maximum absolute velocity, which was 83 cm/s in the simulated time window.

G. In Vivo Feasibility Study

Single and multi-angle plane wave acquisition sequences were implemented on a Verasonics Vantage system (Verasonics Inc., Kirkland, USA), and utilized to obtain channel data

TABLE IV
ALIASING PATTERNS HIGHLIGHTED (RED) IN FIG. 5

TxRx	Set nr.	Aliasing pattern	$\lvert r_i - r_j \rvert$	B_{ij}
1	18 **186**	[0, -1, -1, -1, -2] **[-2, -2, -1, 0, 0]**	$9.7 \cdot 10^{-17}$	$2.9 \cdot 10^{-16}$
4	18 **186**	[-2, -2, -1, 0, 0] **[0, -1, -1, -1, -2]**	0.26	0.44
5	14 **1969**	[-2, -2, -2, -2, -1, -1, -1] **[0, 0, -1, -1, -1, -1, -2]**	0.48	0.66

from the carotid arteries of healthy volunteers. Two linear probes were used, resulting in different *in vivo* imaging setups with the same Doppler PRF, but different Nyquist velocities. Beamforming was performed using the same in-house code as used for flow simulations, and a continuous acquisition enabled the use of a 92 tap Finite Impulse Response (FIR) filter for clutter rejection, with a −6 dB cutoff of 1.5 cm/s. Further specifications of acquisition and processing can be found in Table II.

III. RESULTS

A. Transmit–Receive Pattern Design

The minimum B_{ij} parameter was used to make aliasing-resistant transmit–receive patterns for varying numbers of transmit and receive directions. Seven transmit–receive patterns were selected for further evaluation and are shown in Table III. Patterns 1–3 are examples of nonoptimized transmit–receive patterns, whereas patterns 4–7 are examples of patterns with high aliasing resistance. Given the restrictions in Section II-D, pattern 4 yields the most aliasing-resistant setup utilizing 3 transmit and 5 receive angles, whereas patterns 5, 6, and 7 yield the most aliasing-resistant setups utilizing 7 receive angles and 3, 2, and 1 transmit angles, respectively. Table III (right column) contains the corresponding minimum values of B_{ij}, which were calculated using the method described in Section II-D.

For transmit–receive patterns 1–3, min B_{ij} is close to zero, and notably this leads to a very low aliasing resistance independently of the increasing number of transmit–receive pairs (5, 7, and 9). For the transmit–receive patterns that have been optimized with respect to aliasing resistance (patterns 4–7), min B_{ij} is significantly larger. Note that the transmit–receive patterns with seven angle pairs (5–7), all have equal aliasing resistance in terms of the min B_{ij} parameter. However, the transmit–receive setups differ in the number of plane wave transmissions, which has an impact on the SNR of the coherent compounding image utilized for BM. The use of a single transmit direction (pattern 7) also results in a reduced Doppler angle span.

B. Aliasing-Resistant Versus Nonoptimized TxRx Patterns

Fig. 4 provides an overview of the normalized rms error of v_x and v_z for the two simulation cases utilizing the TxRx patterns listed in Table III. The channel data blood SNR is −5 dB. In Case 1, where only single-wrap aliasing is present, the choice of TxRx pattern does not have a significant impact on the robustness of the velocity estimates. However, in Case 2, there are large differences in the rms errors for

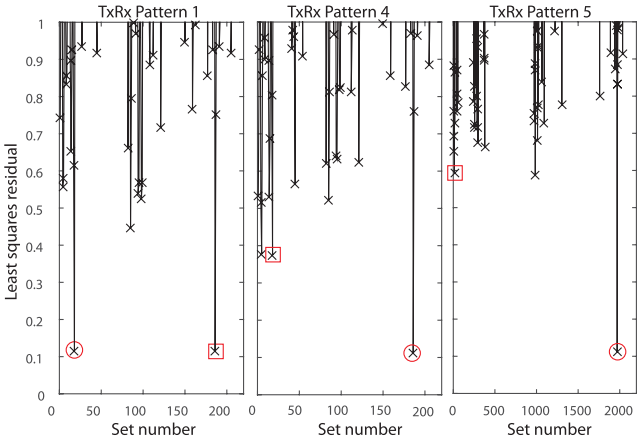

Fig. 5. Least squares residuals in a single image point for the transmit–receive patterns 1, 4, and 5 as a function of aliasing pattern set number. The two smallest residuals are highlighted in red circles (selected aliasing pattern) and red squares (closest competitor). Note that the y-axis has been shortened.

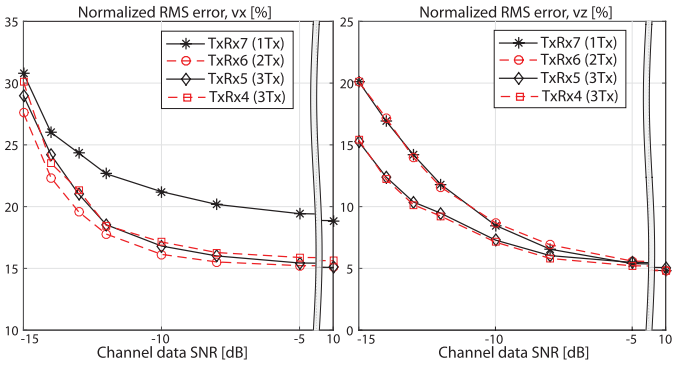

Fig. 6. Performance of the aliasing-resistant transmit–receive patterns in different SNR conditions using the low PRF simulation case. Note that the vertical axes are different in the two panels.

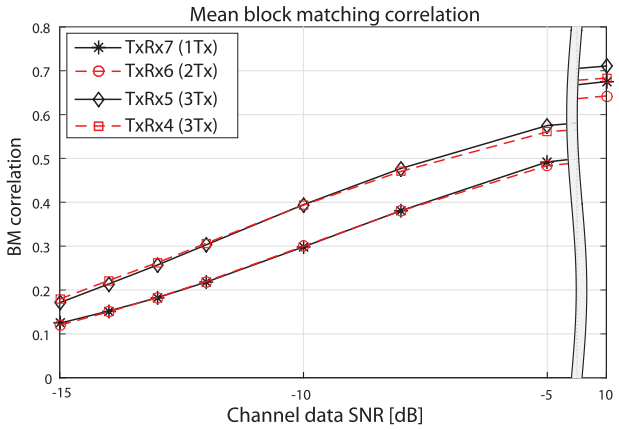

Fig. 7. Mean BM correlation values taken over all pixel values for the selected vector velocity candidates.

the different TxRx patterns, demonstrating that the choice of transmit–receive pattern rather than the number of transmit–receive angles is most important for robust velocity estimation in the presence of higher order aliasing. The lowest rms errors are obtained when regions of higher order aliasing are robustly detected. Patterns 4–7, which fulfill the requirements described in Section II-D, all display a high aliasing resistance. For these patterns, the error in v_z is 5% both in the low PRF

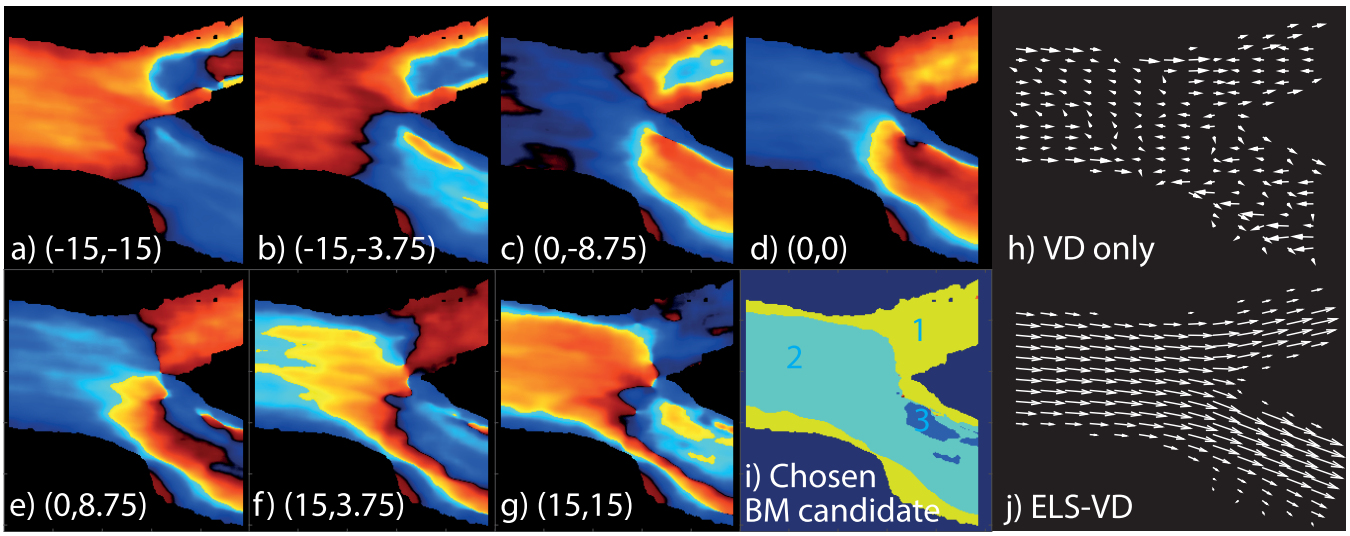

Fig. 8. (a)–(g) Individual color flow images from the carotid artery bifurcation simulation using a low PRF (2 kHz). Transmit and receive angle pairs are given in parentheses. All angle pairs contain single-wrap aliasing and one pair double-wrap aliasing. Panel (h) shows the estimated velocity vectors when utilizing regular least squares VD. In the proposed method, the output of the least squares VD is a small number of velocity vectors for each pixel (e.g., 5), sharing the same minimum residual. BM is then utilized to choose the correct velocity vector candidate. Panel (i) shows where the BM step has corrected the temporary vector velocity estimate. Panel (j) shows the final vector velocity field using the proposed method.

and in the high PRF case. For TxRx patterns 4–6, the error in v_x is 15% in the low PRF case, and smaller in the high PRF case. TxRx pattern 7 has a reduced Doppler angle span, which is reflected in the larger rms values for the horizontal velocity component. In this analysis, no correlation threshold was applied to exclude erroneous estimates. The large rms errors found when using the transmit–receive patterns 1–3 in the simulation Case 2 (low PRF), are caused primarily by erroneous velocity estimation in the regions with multiple aliasing. This result corresponds well with the low values of the minimum B_{ij}, as shown in Table III.

To understand the importance of the parameter B_{ij}, it is useful to study the aliasing pattern selection in a single image pixel containing multiple aliasing. Fig. 5 shows the least squares residuals as a function of aliasing pattern set number for one such pixel, using TxRx patterns 1, 4, and 5. The chosen aliasing pattern for each transmit–receive design is circled in red, whereas its closest competitor is highlighted using a red square. Using TxRx pattern 1 (left panel), we see that the two smallest residuals are (approximately) equal, and an erroneous aliasing pattern is in fact selected in this case. This behavior is representative also for TxRx 2 and 3, and is the origin of the large rms errors seen in Fig. 4. TxRx patterns 4 and 5 are on the other hand chosen to have as large minimum B_{ij} as possible. For these setups, we see that the residuals of the closest competitors increase with increasing B_{ij}, yielding a more robust selection of the correct aliasing pattern. The highlighted aliasing patterns in Fig. 5 are shown in Table IV, with the difference in residuals and the corresponding B_{ij}. The values of $|r_i - r_j|$ are bounded by B_{ij}, as predicted by the theory presented in Section II-B.

C. Robustness of the ELS-VD Method

Fig. 6 shows the performance of ELS-VD in the presence of higher order aliasing utilizing three, two, and single plane wave transmissions. The left panel shows the normalized rms errors in the lateral velocity component as a function of the channel data blood SNR. Whereas the aliasing-resistant setups with two and three plane wave transmissions have similar performance, the single plane wave transmission setup (TxRx7) with its decreased Doppler angle span yields a larger rms value for all the SNR scenarios. Fig. 6 (right panel) shows the normalized rms errors in the vertical velocity component. Here, the transmit–receive TxRx patterns with three transmit angles perform better than those with two and one plane wave. The difference in normalized rms error between the two groups also increases with decreasing SNR.

Fig. 7 shows the mean BM correlation value taken over all pixels for the selected vector velocity candidates. There is a significant increase in the correlation values when utilizing three transmit angles as compared with utilizing only two or one. As the BM step specifically impacts the vertical velocity estimation, these results correspond well with the rms errors shown in Fig. 6 (right panel).

Fig. 8, panels a) to g) show individual color flow images obtained for simulation Case 2 (higher order aliasing present), utilizing TxRx 5 and a channel data SNR of -5 dB (8 dB after coherent compounding with three transmit angles). The estimated vector velocity field with and without aliasing correction is shown to the right. In this case, 85% of all the velocity estimates are aliased in one or more TxRx pairs, with double-wrap aliasing in pair g) ($3v_{\mathrm{Nyq}} \leq |v_{\mathrm{Dop}}| \leq 5v_{\mathrm{Nyq}}$). Fig. 8(h) shows the estimated velocity vectors when utilizing regular least-squares VD without aliasing correction. In the proposed ELS-VD method, the output of the least squares step is not one single velocity vector, but a small number of velocity vectors for each pixel (e.g. 5), sharing the same minimum residual. BM is then utilized to choose the correct velocity vector candidate. Fig. 8(i) shows which vector velocity candidates were chosen by the BM step in this example. In the yellow area (1), there is no negative

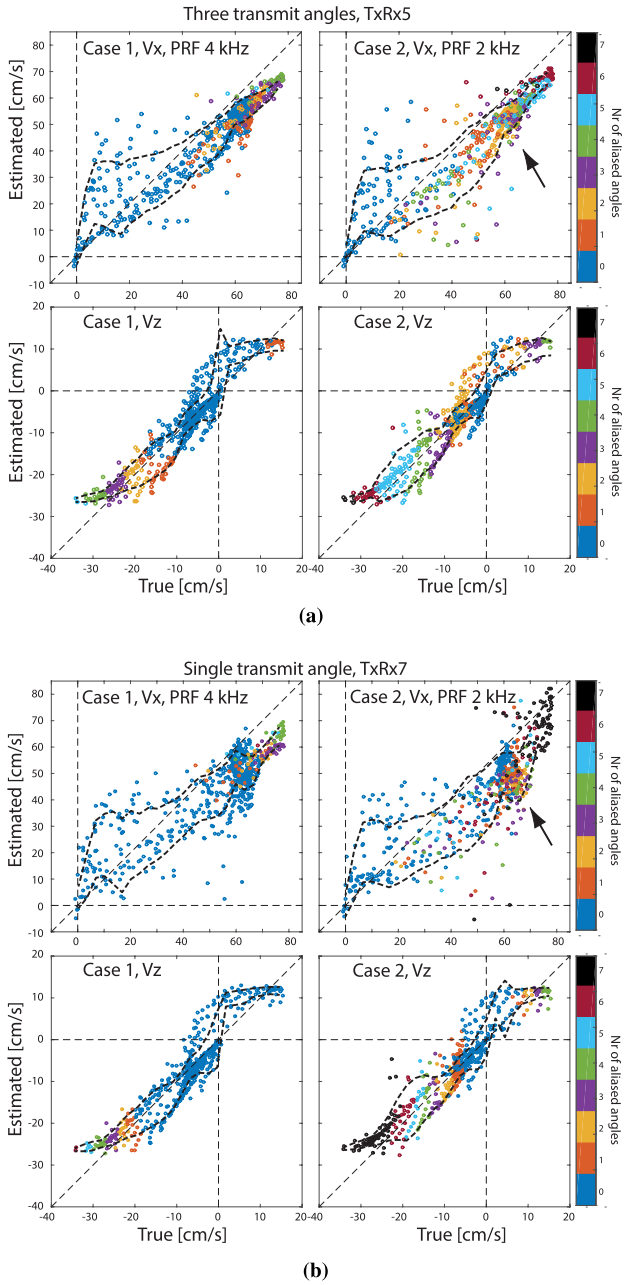

Fig. 9. Scatter plots showing true versus estimated velocity using the aliasing-resistant transmit–receive patterns. In plot (a) three transmits are used, whereas in plot (b) a single transmit is used. Colors represent the number of Doppler estimates that are aliased at each image pixel according to the true velocity field. Black arrows indicate the regions with high point density, which have a large impact on the rms error.

aliasing in any of the transmit–receive pairs (all elements of $g_i \geq 0$), whereas in the cyan (2) and blue (3) regions, there are Doppler estimates with single-wrap and double-wrap negative aliasing, respectively. Fig. 8(j) shows the final vector velocity field using the proposed method.

Fig. 9(a) shows scatter plots of true versus estimated velocity for the two simulation cases, only single-wrap aliasing (left), and both single- and double-wrap aliasing (right) utilizing three transmit angles TxRx 5. Each point represents the velocity in one image pixel, and except for decimating with a factor of 50, all the velocity estimates are included. The color provides information about the true

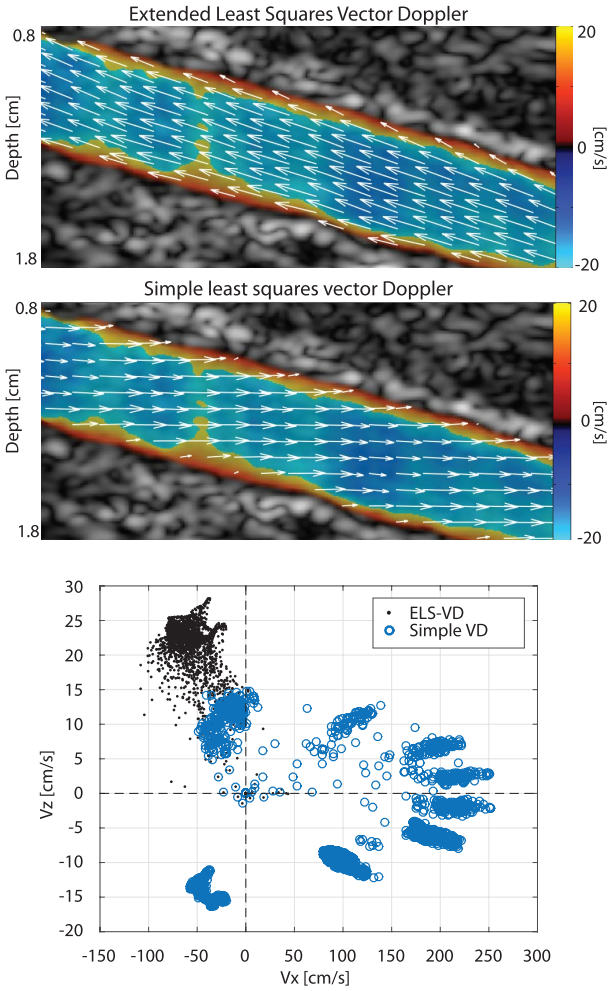

Fig. 10. Common carotid artery of a healthy volunteer imaged in peak systole utilizing a single plane wave transmission angle. Aliasing-resistant vector velocity estimates are obtained utilizing ELS-VD with transmit–receive pattern 7. The scatter plot shows the horizontal and vertical velocity estimates from simple least squares VD (blue circles) and ELS-VD (black dots).

velocity component along each of the seven unique two-way Doppler angles; Blue color means that all the components are below the Nyquist limit, whereas black color means that in the true velocity field all the seven velocity components are above the Nyquist limit. The dashed, black curves represent estimated mean velocity $\pm$ standard deviation with velocity bins of 2 cm/s. The black arrow points to a region with high point density, which has large impact on the rms error (Fig. 6). As seen in Fig. 9(b), the estimator is still aliasing resistant using only a single transmit angle (TxRx7). However, the variance in the lateral velocity component is increased, especially in the region indicated by the black arrow.

D. Single Plane Wave Transmission Angle: In Vivo

Fig. 10 shows the common carotid artery of a healthy volunteer, imaged using the L11 setup. Estimated vector velocities are superimposed on the color flow image. As seen in the top panel aliasing-resistant vector velocity estimates can be obtained also *in vivo* utilizing only a single plane wave transmission. The frame is taken from peak systole, and as demonstrated by the color flow image in the background, most

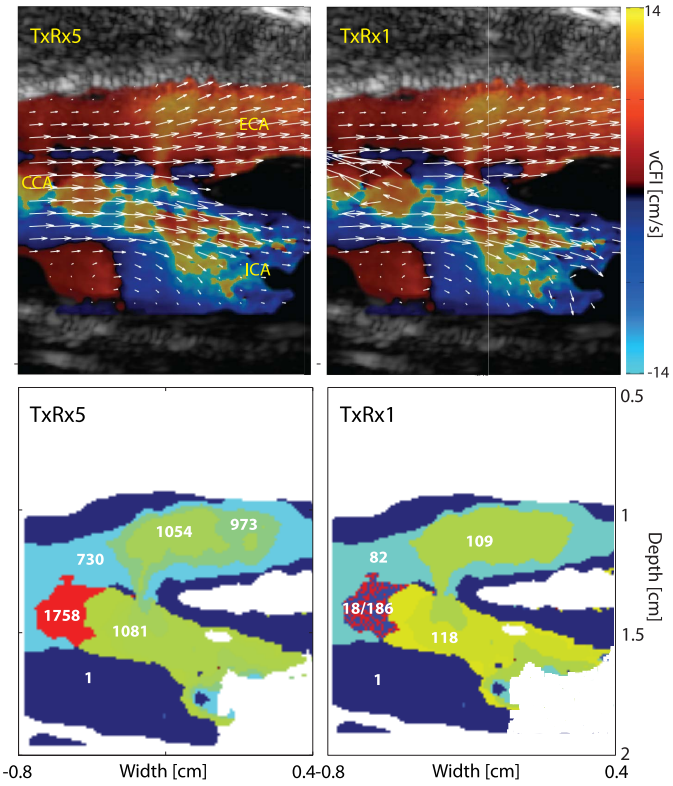

Fig. 11. Top panels: flow in the carotid bifurcation of a healthy volunteer in systole using transmit–receive pattern 5 (left) and 1 (right) from Table III. Bottom panels: depiction of the aliasing patterns found when using TxRx5 (high aliasing resistance) and TxRx1 (low aliasing resistance). Numbers within color patches are the indices of distinct sets of the candidate vectors S_i (see Section II-B).

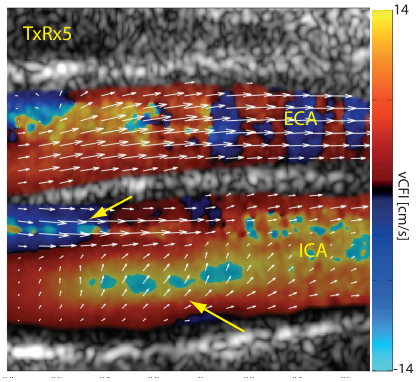

Fig. 12. Flow in the external carotid artery (ECA) and ICA of a healthy volunteer in systolic deceleration using transmit–receive pattern 5. Yellow arrows: two distinct flow patterns in the ICA.

of the flow pixels are aliased even with no steering. TxRx 7 is used, which means that the flow measurement vector consists of seven unique Doppler measurements for each pixel—all with possible aliasing. The scatter plot shows the horizontal and vertical velocity estimates from all pixels in the color flow region. Aliasing-resistant estimates utilizing the proposed method are shown in black, whereas simple least squares regression VD estimates are shown in blue.

E. Multiangle Plane Wave Transmission: In Vivo

Figs. 11 and 12 (top panels) show estimated vector velocity flow fields from two different image planes of a carotid artery bifurcation, imaged using the L12 setup. For the image plane shown in Fig. 11, notable flow features include rotational flow in the bulb region and high velocities close to the flow divider going into the internal carotid artery (ICA). Fig. 12 shows a slightly different image plane of the same carotid bifurcation (systolic deceleration). In the ICA two blood flow patterns dominate; a high velocity stream close to the proximal wall in addition to indications of helical flow. The background images are the coherent compounding B-mode and color flow images, whereas the 2-D flow field is the result of the proposed ELS-VD technique. Using TxRx pattern 5, aliasing-resistant vector velocity estimates are obtained in all parts of the image, even though the high transmit frequency and low PRF utilized in the L12 imaging setup result in a very low Nyquist limit and a large portion of the Doppler measurements being aliased. The high degree of aliasing is clearly shown in Fig. 11 (bottom panels). These figures show aliasing patterns yielding the estimated vector flow fields shown in the corresponding upper panels. Each color represents a unique S_i index, corresponding to a unique set of candidate velocity vectors. Some patches are numbered to highlight different pattern regions. The number 1 (dark blue color) represents a region without aliasing in any of the Doppler measurements. In all other regions, one or more of the Doppler measurements are aliased. Successful pattern mapping is characterized by the presence of patches with only a single color (left panel). As seen in the image to the right, the use of TxRx pattern 1 results in a region in front of the flow divider where the selected aliasing pattern rapidly alternates between $[1, 0, 0, 0, -1]$ and $[-1, -1, 0, 1, 1]$, with corresponding $B_{ij} = 2.9 \cdot 10^{-16}$. Selecting an erroneous aliasing pattern in this manner leads to a BM search based on the wrong set of candidate vectors, eventually resulting in erroneous velocity estimates and/or vector velocity dropouts due to low correlation values. This is seen in Fig. 11 (top right image), where the vector field is shown without correlation thresholding to also display the estimates resulting from erroneous aliasing pattern detection.

Fig. 13 shows the estimated vector velocity flow field in the carotid bifurcation using the L11 probe in systolic deceleration, with good view of both the bulb region (swirling flow) and the two branches of the carotid artery. See also the supplementary video for a full cardiac cycle. To add some quantitative measures of the flow, two sample volumes are indicated: 1) just before the flow divider and 2) within the high velocity stream going into the ICA. Fig. 14 shows PW Doppler spectra from these two sample volumes in addition to the corresponding VD velocity estimate (white line). PW Doppler spectra were generated from the TxRx pair yielding the best estimated beam-to-flow angle and were (automatically) angle corrected to give absolute velocity estimates. Red dashed lines indicate multiples of the (angle corrected) Nyquist limit, showing that the suggested ELS-VD algorithm is robust in terms of aliasing. However, as can be seen in Fig. 14 (right panel), clutter filtering affects the Doppler signal at multiples

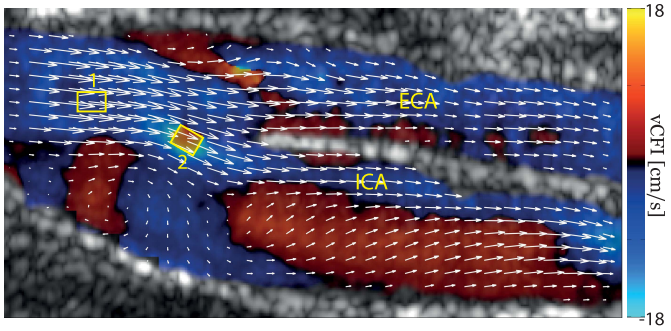

Fig. 13. Depiction of blood flow in the carotid bifurcation of a healthy volunteer using the L11 probe. See also supplementary video. Two sample volumes are indicated, which are further used for the comparison of PW Doppler spectra and velocity magnitude estimates in Fig. 14. The image frame shows the blood flow patterns in the systolic deceleration phase.

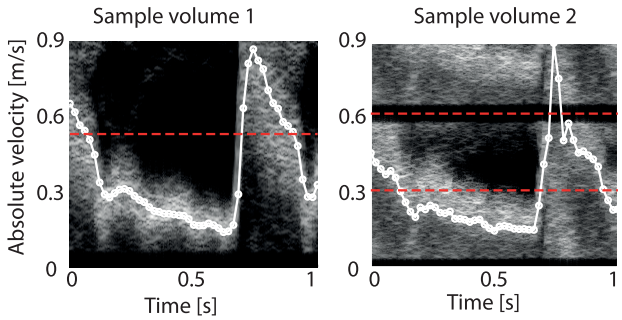

Fig. 14. PW Doppler spectra from sample volumes 1 and 2 in Fig. 13, in addition to the vector velocity estimate (white line). The velocity axes are corrected with the estimated beam-to-flow angles, 110 and 130 degrees for sample volumes 1 and 2, respectively. Red dashed lines: multiples of the (angle corrected) Nyquist velocity, in which the beam direction is 18 cm/s. Dynamic range is 30 dB.

of $2 \times v_{\mathrm{Nyq}}$. In this example, the missing flow signal in this region results in a negative bias in the VD estimate at $t = 0.78\ s$.

IV. Discussion

The ELS-VD method for robust, aliasing-resistant 2-D vector velocity imaging has been presented, extending previous work in the field [19]. The method utilizes a combination of least squares regression of Doppler autocorrelation estimates and BM of blood speckle to obtain the velocity vectors. Least squares regression is used to obtain a set of vector velocity candidates and aliasing patterns, whereas BM is used to choose the correct vector velocity candidate. The transmit–receive angle combinations are specifically designed to minimize the probability of selecting the erroneous aliasing patterns. The method can be used for aliasing-resistant vector velocity estimation in setups using a single transmit aperture, as well as in dual- or multitransmit beam setups.

It was shown that straightforward implementation of least squares VD as presented in [19] is not sufficient to reliably distinguish all the possible aliasing patterns for higher order aliasing. More specifically, in Section II-B, it was shown that as long as $\cos \alpha_n \approx 1$ for all steering angles α_n, some aliasing patterns belong to a set of several patterns that are in practice indistinguishable using VD only. The use of some method other than least squares regression is necessary to distinguish the patterns within each set.

Ambiguities may arise also between the aliasing patterns that are not in the same set because of small differences in the least squares residuals. In the presence of noise, this may cause selection of the wrong aliasing pattern, resulting in a BM search evaluating only the erroneous velocity vector candidates. For a given combination of transmit and receive angles, we have shown that the ability to discern different aliasing patterns and choose the correct one can be quantified using a single parameter $\min B_{ij}$, which is described in Section II-B and II-C. The fact that the difference in least squares residuals between the correct estimate $\boldsymbol{v}_i$ and its closest competitor $\boldsymbol{v}_j$ is equal to B_{ij} in the noiseless case means that the setup becomes more resilient to variance and bias in the autocorrelation estimates if $\min B_{ij}$ is large. Note that the aliasing resistance of a sequence is not directly dependent on properties such as angle span and correlation between the measured signals, but is a mathematical property of the matrix $\mathbf{A}$ given in (2).

As shown by the results in Section III-B, proper selection of the transmit and receive angles as described in Section II-D significantly increases the probability of choosing the correct set of velocity vector candidates, whereas this probability is not necessarily increased by simply increasing the number of TxRx pairs. This is clearly seen in Fig. 4, where TxRx patterns 1 and 3 give equally poor results, even though pattern 3 is based on nine unique autocorrelation estimates, and pattern 1 is based on only 5. Patterns 4 and 5 on the other hand both perform well, using only 5 and 7 autocorrelation estimates per pixel, respectively.

The accuracy of the method was quantified using a simulation of flow and tissue scatterers in a patient specific carotid artery bifurcation model. Simulation results indicate that the proposed technique provides aliasing-resistant velocity estimates for the setups using one, two, and three transmission directions, as shown in Figs. 6 and 9(a) and (b). It is also robust in terms of SNR, as there is only a slight increase in the rms error when the channel data SNR is decreased from 10 dB to -5 dB. However, for very low signal-to-noise levels (below -8 dB), a significant degradation of the velocity estimates is observed, due to the erroneous selection of aliasing patterns.

Erroneous selection of the aliasing patterns may be due to the method selecting the wrong set in the least squares regression step, or the wrong velocity vector candidate in the BM step. However, the results in Fig. 6 indicate that the BM step is less robust for low SNR than the least squares regression step. One indicator of this is that TxRx pattern 4 performs similar to TxRx pattern 5 for all SNRs, even though pattern 5 should be more robust to noise, because the minimum B_{ij} is significantly higher. This behavior indicates that they are both selecting the correct aliasing sets, and that the performance degradation seen for low SNRs is primarily due to a breakdown in the BM step, which due to the equal number of transmit angles would affect both transmit–receive patterns similarly.

Breakdown of the BM step also explains the increased error in the vertical velocity estimates observed for low SNRs when using one or two transmissions, as the correlation values obtained using these setups (Fig. 7) are lower than the setups using three transmissions. Notably the setup with two transmit angles achieved similar correlation values as the setup using a single transmit angle, and also the same vertical rms errors. The lacking increase in correlation between one and two transmit angles is partially explained by the high velocities in the simulated Doppler frame, in which case the SNR gain from coherent compounding is reduced if motion compensation is not applied [24], [25]. This effect is further amplified by the simulation setup originally designed for three angles, so that the time between successive transmissions corresponds to a 3 kHz maximum PRF for the two-angle setup compared with a 6 kHz maximum PRF for the three-angle setup.

Even in adequate SNR conditions, BM may still fail due to strong spatial velocity gradients, high velocity flow or out-of-plane movement, resulting in signal correlation below the acceptable threshold. The use of a correlation threshold is therefore important to ensure that valid velocity estimates are displayed.

The transmit–receive patterns used in this paper were designed to maximize the aliasing resistance, and are therefore not necessarily optimal for achieving the most accurate velocity estimates. Some properties of the TxRx patterns, which are not thoroughly discussed in this paper, also influence the accuracy of the VD estimates. For example, several of the transmit–receive patterns include overlapping receive apertures from the same transmission, which would result in correlated observations being used as input to the least squares step. In addition, the use of large steering angles decreases the variance in the lateral velocity estimates, but may also cause grating lobes in the low resolution images, depending on the probe geometry. The influence of the angle span on the accuracy can be observed in Fig. 6 (left panel), as the setup using a single plane wave yields significantly higher rms errors in the lateral velocity estimates.

Finally, observations from different angles may have different bias and variance due to clutter filtering and different effective transit times. Although clutter filtering did not seem to have a significant impact on aliasing correction in this paper, variance differences due to clutter filtering may be corrected for by using a different weighting matrix $\boldsymbol{W}$ than the identity matrix. However, as the current aim was to develop a robust means of resolving aliasing ambiguities, the details of the implementation of such a weighting function was considered out of the scope of this paper. It should be noted that the transmit–receive pattern optimization described in Section II-D was not dependent on the measured data, and thus the selected transmit–receive pattern might not be the most aliasing-resistant choice in all pixels if the autocorrelation estimates are weighted dynamically. In theory, it is possible to dynamically select the receive steering angles for each pixel, but assuming a uniform weighting when selecting the transmit–receive pattern is a reasonable way of producing a computationally feasible implementation.

Compared with cross-beam VD, multi-angle VD produces more robust and accurate blood velocity measurements. The use of two or more transmit angles reduces the variance in the lateral estimates and the influence of dropouts caused by clutter filtering. On the other hand, when interleaving the firings from different angles, the reduced PRF makes the sequence more prone to aliasing. In this paper, we have shown that the advantages of multi angle VD may be obtained while simultaneously solving the aliasing problems. Alternatively, the sequence could have been implemented without interleaving as in [19], firing several successive transmissions from one angle before moving on to the next angle and regaining the maximum Doppler PRF. In this case, compounding of plane waves from different angles would be impossible, but the BM step could be performed on the images generated from each transmit angle separately and averaged. The main disadvantage of this alternative is that it yields a packet acquisition in which the ensemble size determines a tradeoff between accurate measurements of slow flow, and ability to capture rapid accelerations.

Another potential advantage of interleaving firings from different angles is that the same sequence may be used for coherent compounding and B-mode imaging. It should be noted that the TxRx patterns that are optimally aliasing-resistant are not necessarily optimal for the quality of the compounded B-mode images. In addition, high center frequencies and short pulse lengths are preferred in B-mode imaging to improve resolution, whereas the low center frequencies and long pulse lengths are preferred in Doppler imaging to increase penetration, SNR, and clutter filter efficiency.

We include in the following a brief comparison between the method presented in this paper and other alternatives for aliasing-resistant vector velocity imaging. The accuracy and robustness of the vector velocity estimates in this paper is, similar to both the conventional cross-beam VD and the work of Yiu *et al.* [10], primarily dependent on the bias and variance of the autocorrelation estimates and the span of the two-way Doppler angles. This is in contrast to for example speckle tracking and directional beamforming, which depend on spatial correlation rather than estimation of Doppler shifts. These methods are therefore more dependent on high spatial resolution and low spatial velocity gradients, whereas the Doppler methods become more accurate when using longer pulses, yielding a lower resolution. In one study comparing the cross-beam VD and speckle tracking techniques, it was concluded that VD provided a more accurate axial estimate, whereas the two methods had similar performance for the lateral velocity components [26]. In another such study, it was found that the speckle tracking was more sensitive to low SNR, but yielded more robust velocity estimation in the transition band of the clutter filter [27].

The main difference between our method and [10] is that rather than performing aliasing correction on the signal from each angle separately, the proposed method determines the degree of aliasing for all the Doppler signals simultaneously based on measurements from all the receive angles. Using information from all angles should result in a more robust estimate of the degree of aliasing, but the underlying assumption is

that the signal from all the angles represents the same spatial region, which depends on spatial resolution. A quantitative study would be necessary to further compare the performance of the aliasing-resistant technique presented in this paper to speckle tracking and the methods proposed in [10] and [18].

As a final note, use of the proposed method is more challenging in for example cardiac imaging, because of the smaller transducer aperture and deeper regions of interest. Aliasing-resistant velocity estimation in cardiac applications can, however, be achieved using methods not based on multi-angle Doppler information, like speckle tracking or staggered PRF.

V. Conclusion

An aliasing-resistant vector velocity imaging technique has been proposed, combining least squares vector Doppler with block matching to resolve ambiguities. It was shown that careful selection of the transmit and receive angles can be used to increase the robustness of the aliasing correction step, and that this is more effective than increasing the number of transmit–receive combinations. It was found that the proposed method produces reliable vector velocity estimates for velocities up to five times the Nyquist limit, and thus significantly extends the measurable velocity span of vector Doppler imaging.

References

[1] B. Dunmire, K. W. Beach, K.-H. Labs, M. Plett, and D. E. Strandness, Jr., "Cross-beam vector Doppler ultrasound for angle-independent velocity measurements," *Ultrasound Med. Biol.*, vol. 26, no. 8, pp. 1213–1235, Oct. 2000.

[2] T. Tamura, R. S. C. Cobbold, and K. W. Johnston, "Determination of 2-D velocity vectors using color Doppler ultrasound," in *Proc. IEEE Ultrason. Symp.*, Dec. 1990, pp. 1537–1540.

[3] M. Scabia, M. Calzolai, L. Capineri, L. Masotti, and A. Fort, "A real-time two-dimensional pulsed-wave Doppler system," *Ultrasound Med. Biol.*, vol. 26, no. 1, pp. 121–131, 2000.

[4] S. Xu, H. Ermert, and R. Hammentgen, "Phased array pulse Doppler tomography," in *Proc. IEEE Ultrason. Symp.*, Dec. 1991, pp. 1273–1276.

[5] J. A. Jensen and P. Munk, "A new method for estimation of velocity vectors," *IEEE Trans. Ultrason., Ferroelectr., Freq. Control*, vol. 45, no. 3, pp. 837–851, May 1998.

[6] T. A. Maniatis, R. S. C. Cobbold, and K. W. Johnston, "Two-dimensional velocity reconstruction strategies for color flow Doppler ultrasound images," *Ultrasound Med. Biol.*, vol. 20, no. 2, pp. 137–145, 1994.

[7] L. N. Bohs, B. J. Geiman, M. E. Anderson, S. M. Breit, and G. E. Trahey, "Ensemble tracking for 2D vector velocity measurement: Experimental and initial clinical results," *IEEE Trans. Ultrason., Ferroelectr., Freq. Control*, vol. 45, no. 4, pp. 912–924, Jul. 1998.

[8] A. J. Jensen and S. I. Nikolov, "Directional synthetic aperture flow imaging," *IEEE Trans. Ultrason., Ferroelectr., Freq. Control*, vol. 51, no. 9, pp. 1107–1118, Sep. 2004.

[9] I. K. Ekroll, A. Swillens, P. Segers, T. Dahl, H. Torp, and L. Lovstakken, "Simultaneous quantification of flow and tissue velocities based on multi-angle plane wave imaging," *IEEE Trans. Ultrason., Ferroelectr., Freq. Control*, vol. 60, no. 4, pp. 727–738, Apr. 2013.

[10] B. Y. S. Yiu, S. S. M. Lai, and A. C. H. Yu, "Vector projectile imaging: Time-resolved dynamic visualization of complex flow patterns," *Ultrasound Med. Biol.*, vol. 40, no. 9, pp. 2295–2309, Sep. 2014.

[11] P. Hoskins, "A comparison of single- and dual-beam methods for maximum velocity estimation," *Ultrasound Med. Biol.*, vol. 25, no. 4, pp. 583–592, 1999.

[12] G.-M. von Reutern *et al.*, "Grading carotid stenosis using ultrasonic methods," *Stroke*, vol. 43, no. 3, pp. 916–921, 2012.

[13] R. Bamler and P. Hartl, "Synthetic aperture radar interferometry," *Inverse Problems*, vol. 14, no. 4, p. R1, 1998.

[14] J. Laroche and M. Dolson, "Improved phase vocoder time-scale modification of audio," *IEEE Trans. Speech Audio Process.*, vol. 7, no. 3, pp. 323–332, May 1999.

[15] A. Shahin, M. Ménard, and M. Eboueya, "Cooperation of fuzzy segmentation operators for correction aliasing phenomenon in 3D color Doppler imaging," *Artif. Intell. Med.*, vol. 19, no. 2, pp. 121–154, 2000.

[16] S. Muth, S. Dort, I. A. Sebag, M.-J. Blais, and D. Garcia, "Unsupervised dealiasing and denoising of color-Doppler data," *Med. Image Anal.*, vol. 15, no. 4, pp. 577–588, 2011.

[17] A. M. Yatchenko, A. S. Krylov, V. A. Sandrikov, and T. Y. Kulagina, "Regularizing method for phase antialiasing in color Doppler flow mapping," *Neurocomputing*, vol. 139, pp. 77–83, Sep. 2014.

[18] D. Posada *et al.*, "Staggered multiple-PRF ultrafast color Doppler," *IEEE Trans. Med. Imag.*, vol. 35, no. 6, pp. 1510–1521, Jun. 2016.

[19] J. Flynn, R. Daigle, L. Pflugrath, K. Linkhart, and P. Kaczkowski, "Estimation and display for vector Doppler imaging using planewave transmissions," in *Proc. IEEE Ultrason. Symp.*, Oct. 2011, pp. 413–418.

[20] J. Flynn and R. E. Daigle, "Estimation and display for vector doppler imaging using plane wave transmissions," U.S. Patent 9 192 359, Nov. 24, 2015.

[21] A. Swillens, G. De Santis, J. Degroote, L. Lovstakken, J. Vierendeels, and P. Segers, "Accuracy of carotid strain estimates from ultrasonic wall tracking: A study based on multiphysics simulations and *in vivo* data," *IEEE Trans. Med. Imag.*, vol. 31, no. 1, pp. 131–139, Jan. 2012.

[22] J. A. Jensen, "Field: A program for simulating ultrasound systems," in *Proc. 10th Nordicbaltic Conf. Biomed. Imag.*, vol. 4. 1996, pp. 351–353.

[23] A. Swillens, J. Degroote, J. Vierendeels, L. Lovstakken, and P. Segers, "A simulation environment for validating ultrasonic blood flow and vessel wall imaging based on fluid-structure interaction simulations: Ultrasonic assessment of arterial distension and wall shear rate," *Med. Phys.*, vol. 37, no. 8, pp. 4318–4330, 2010.

[24] B. Denarie *et al.*, "Coherent plane wave compounding for very high frame rate ultrasonography of rapidly moving targets," *IEEE Trans. Med. Imag.*, vol. 32, no. 7, pp. 1265–1276, Jul. 2013.

[25] I. K. Ekroll, M. M. Voormolen, O. K.-V. Standal, J. M. Rau, and L. Lovstakken, "Coherent compounding in Doppler imaging," *IEEE Trans. Ultrason., Ferroelectr., Freq. Control*, vol. 62, no. 9, pp. 1634–1643, Sep. 2015.

[26] A. Swillens, P. Segers, H. Torp, and L. Lovstakken, "Two-dimensional blood velocity estimation with ultrasound: Speckle tracking versus crossed-beam vector Doppler based on flow simulations in a carotid bifurcation model," *IEEE Trans. Ultrason., Ferroelectr., Freq. Control*, vol. 57, no. 2, pp. 327–339, Feb. 2010.

[27] S. Fadnes, I. K. Ekroll, S. A. Nyrnes, H. Torp, and L. Lovstakken, "Robust angle-independent blood velocity estimation based on dual-angle plane wave imaging," *IEEE Trans. Ultrason., Ferroelectr., Freq. Control*, vol. 62, no. 10, pp. 1757–1767, Oct. 2015.

Ingvild Kinn Ekroll (S'12–M'13) was born in Ålesund, Norway, in 1984. She received the master's degree in biophysics and medical technology and the Ph.D. degree in medical technology from the Norwegian University of Science and Technology (NTNU), Trondheim, Norway, in 2009 and 2013, respectively.

She holds a postdoctoral position with the Department of Circulation and Medical Imaging, NTNU, where she is involved in ultrasound signal processing and visualization for blood flow imaging applications.

Jørgen Avdal (M'15) was born in Årdal, Norway, in 1984. He received the master's degree in industrial mathematics and the Ph.D. degree in medical technology from the Norwegian University of Science and Technology (NTNU), Trondheim, Norway, in 2009 and 2013, respectively.

He holds a postdoctoral position with the Department of Circulation and Medical imaging, NTNU, where he is involved in ultrasound signal processing, blood flow imaging, and spectral Doppler applications.

Abigail Swillens received the master's degree in engineering physics from Ghent University, Ghent, Belgium, in 2006, and the Ph.D. degrees in biomedical engineering from Ghent University and the Norwegian University of Science and Technology, Trondheim, Norway, in 2010.

She is currently an Assistant Professor in medical ultrasound with Ghent University. Her current research interests include multiphysics modeling for the development of cardiovascular ultrasound imaging and investigating image modalities for both blood flow imaging and cardiovascular tissue stiffness assessment.

Hans Torp (M'93) was born in Sarpsborg, Norway, in 1953. He received the M.S. and Dr.Techn. degrees from the Norwegian University of Trondheim (NTNU), Norway, in 1978 and 1992, respectively.

He has been with the Department of Circulation and Medical Imaging, Faculty of Medicine, NTNU, since 1983, where he has been a fulltime Professor, since 1998. His current research interests include stochastic signal/image processing with applications in ultrasonic imaging, Doppler, and color flow imaging.

Lasse Løvstakken (S'05–M'07) was born in Bergen, Norway, in 1976. He received the M.Sc. degree in engineering cybernetics and the Ph.D. degree in medical technology from the Norwegian University of Science and Technology (NTNU), Trondheim, Norway, in 2002 and 2007, respectively.

He is currently a Researcher with the Department of Circulation and Medical Imaging, NTNU. His current research interests include image formation and signal processing, with emphasis on blood flow imaging in diagnostic ultrasound.